Supporting Information for

Transport Properties of Unrestricted Carriers in Bridge-Channel MoS_2 Field-Effect Transistors

Dongri Qiu[1], Dong Uk Lee[2], Chang Soo Park[1], Kyoung Su Lee[1], and Eun Kyu Kim[1,*]

[1]Quantum-Function Research Laboratory and Department of Physics, Hanyang University, Seoul 133-791, South Korea

[2]NAND Development Division, NAND Advanced Product Development, SK Hynix, Icheon 467-734, South Korea

[*]To whom correspondence should be addressed: ek-kim@hanyang.ac.kr

Keywords: Molybdenum disulfide, Field-effect transistor, Bridge-channel, Carrier mobility, Interface density of state

AFM topography of transferred MoS_2 samples

During the devices fabrication, we found that conventional scotch tape-based exfoliation method leaves residuals (like adhesive materials) on the surface of SiO_2. Employing an optimized technique based on PDMS intermediate films to mechanically exfoliate the bulk MoS_2 minimizes the contamination of the samples. Fig. S1 presents optical and AFM images of samples transfer onto SiO_2/Si substrate.

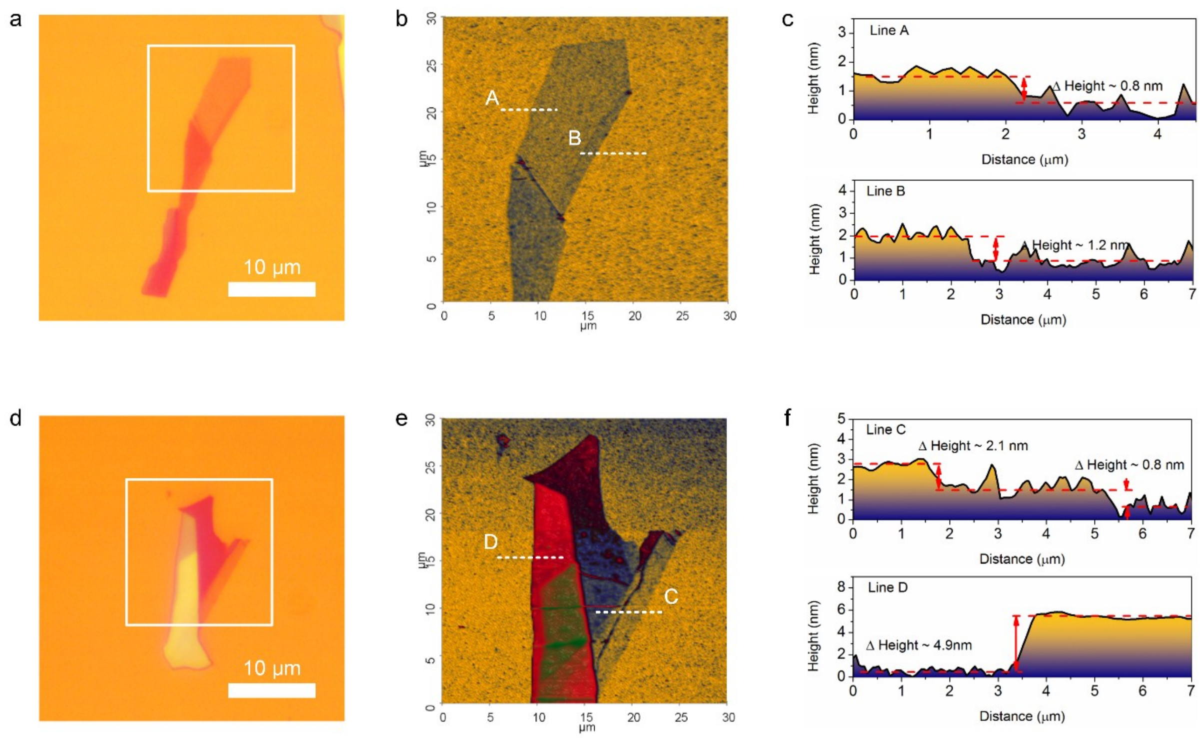

Fig. S1. (a) Optical image of MoS_2 flake deposited on 280-nm-SiO_2/Si substrate. (b) AFM image of the selected area (white box). (c) The corresponding height profiles along the line A (top) and B (bottom). (d)-(f) are optical image, AFM image, and cross-section profile, respectively.

Raman characterizations

The exfoliated MoS_2 samples exhibited two strong signals corresponding to E^1_{2g} (in-plane vibration) and A_{1g} (out-of-plane vibration) mode, as shown in Fig. S2. When reducing the number of MoS_2 layer from bulk to 1L (mono-layer), frequency difference (A_{1g}- E^1_{2g}) changed from 26.4 cm^{-1} to 18.8 cm^{-1}, which is in consistent with other reports. [1, 2]

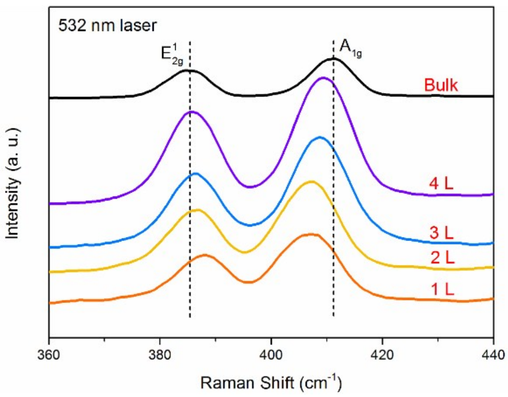

Fig. S2. Raman spectra of various thicknesses (one- to four-layer and bulk) of exfoliated MoS_2 using 532nm laser.

The determination of vacuum gap and capacitance

The transfer of MoS_2 flake on two Au pads (source/drain) usually causes a small displacement toward to the bottom direction, and MoS_2 beam (or channel) is in non-parallel position with respect to bottom substrate, as shown in Manuscript (see Fig. 1). This was confirmed through detail AFM measurement, Fig. 3c shows the cross-sectional profile of MoS_2 beam along the line A in Fig. S3b. As shown in Fig. S3d, the height profile along line B yields a distance of ~40.7 nm. Hence, the minimum distance between MoS_2 and substrate is deduced to be $d_{VA,MIN}$~38 nm (by excluding the thickness of MoS_2). Because of bending nature of MoS_2 beam, it is necessary to calculate the capacitance with small deflection formed in MoS_2 channel. The vacuum gap introduced capacitance C_{VA} can be estimated as following equation.[3]

$$C_{VA}=\varepsilon_r\varepsilon_0/S\int_0^L W/d_{VA}(x)dx \quad (1)$$

Where, S is the area of MoS_2 beam, $d_{VA}(x)$ is the channel length dependent vacuum gap and extracted using sine function a+b*sin*[π(x+c)/d], where the fitting parameters are a=0.0605, b=0.0197, c=0.4517, and d=1.2392. The vacuum capacitance is extracted to be $C_{VA}=1.48\times10^{-8}$ Fcm^{-2}. Then the exact total capacitance is $C_{TOT}=6.72\times10^{-9}$ Fcm^{-2}, since oxide capacitor and vacuum capacitor are in series connection.

To simplify above modeling, alternatively, we used an approximation, i.e. the parallel-palate capacitor model for extracting carrier motilities in this work, in order to avoid overestimation of the mobility (we used a value of $C_{VA}=\varepsilon_0/d_{OX}=2.21\times10^{-8}$ Fcm^{-2}, here d_{OX}~40 nm). It is worth to note that, mobility μ is proportional to $1/C_{TOT}$, and smaller capacitance give rise to higher mobility.

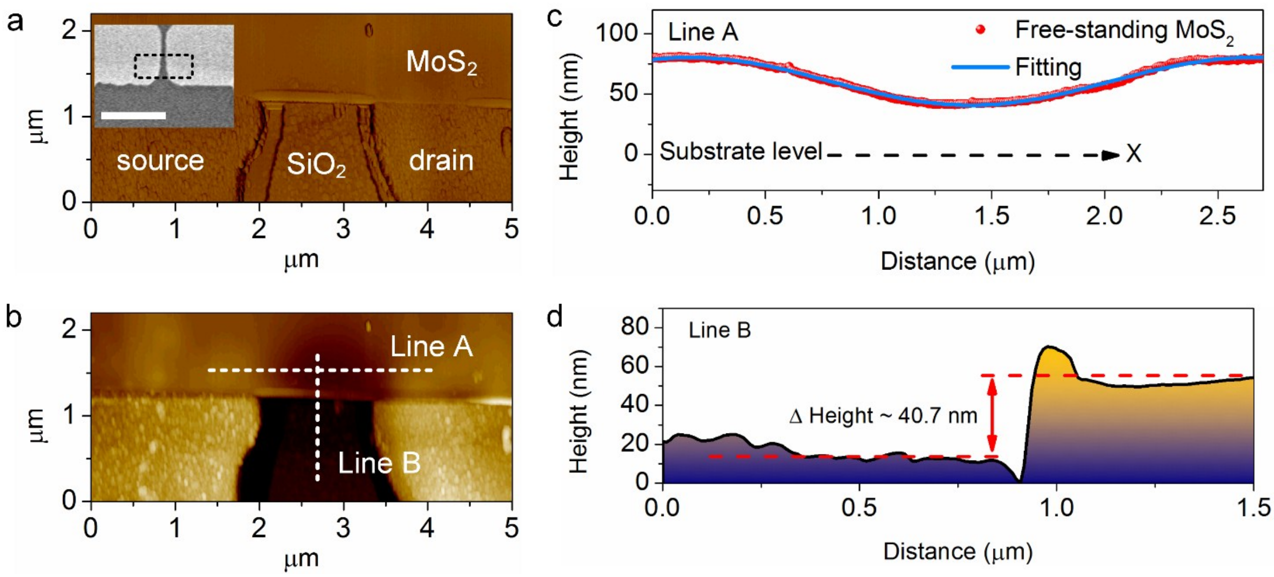

Fig. S3 (a) phase image and (b) AFM topography of the selected area of a device corresponding to the highlighted area in inset of (a) (Inset: low magnification SEM image. Scale bar is 10 μm.). The dashed lines labeled by A and B are perpendicular to each other. The corresponding height profile of the line A and B are given in (c) and (d). Note that the y-axis of (c) and (d) is in nanometer unit.

SEM characterization

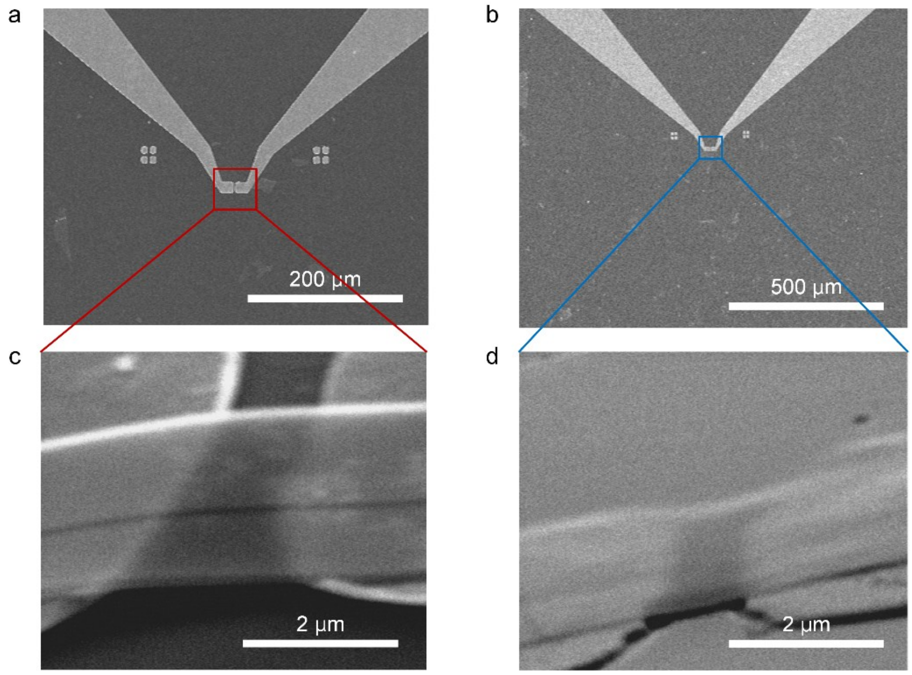

Fig. S4. (a)-(b) SEM images of two MoS_2 transistors with bridge-channel and corresponding magnified SEM images of the selected area (c)-(d).

Linear extrapolation method for determination threshold voltage

Small drain voltage ensures the device operating in the linear region which could neglect series resistance.[4] Threshold voltage V_T is obtained by using linear fit the I_{DS}-V_{BG} curve at linear region. The fitting extrapolate to I_{DS}= 0, and the intercept gate voltage gives V_{BG}' which define zero drain current point as shown in Fig. S2. Substituting V_{BG}' to equation V_T= V_{BG}'-(1/2)V_{DS}. We find threshold voltage of the bridge-channel FET is V_T= -3.23 V.

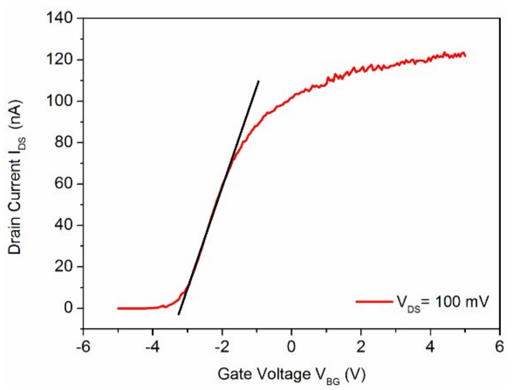

Fig. S5. Threshold voltage determination at low drain voltage (V_{DS}= 100 mV) for the bridge-channel FET by using the linear extrapolation method.

Calculation of contact resistance

The circuit model of series resistance consists of source resistance R_S, drain resistance R_D, and channel resistance R_{CH}, as presented in Manuscript. Generally, the MoS_2 channel conductivity depends on the gate bias V_{BG}, while a large forward V_{BG} results in high electron accumulation at the MoS_2 channel surface. Hence, the channel is regarded as negligible resistance, and all ohmic voltage drops occur at the metal contact associated with series resistance. [5] We assume that a large contribution of series resistance is the contact resistance R_C and neglect the spreading resistance. Based on linear extrapolation of $1/(dI_{DS}/dV_{DS})$ at high gate voltage, the contact resistance roughly estimated is R_C ~250.1 kΩ.

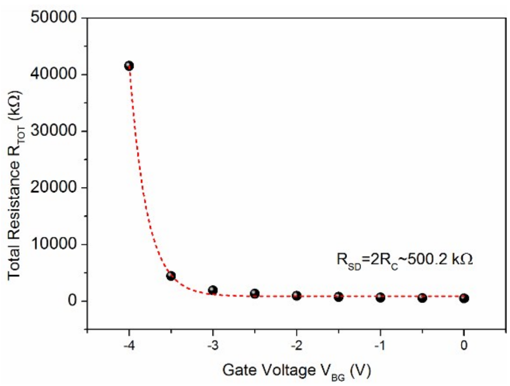

Fig. S6. The total resistance, R_{TOT} as function of gate voltage V_{BG}.

The intrinsic effective mobility

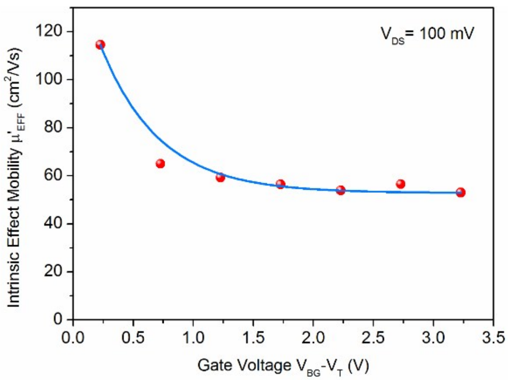

Fig. S7. Intrinsic effective mobility as function of (V_{BG}-V_T) extracted from Equation 1 in Manuscript. The intrinsic effective mobility of the bridge-channel transistor under low drain bias (V_{DS}= 100 mV) to make FET operating at linear regime.

The subthreshold slope extractions

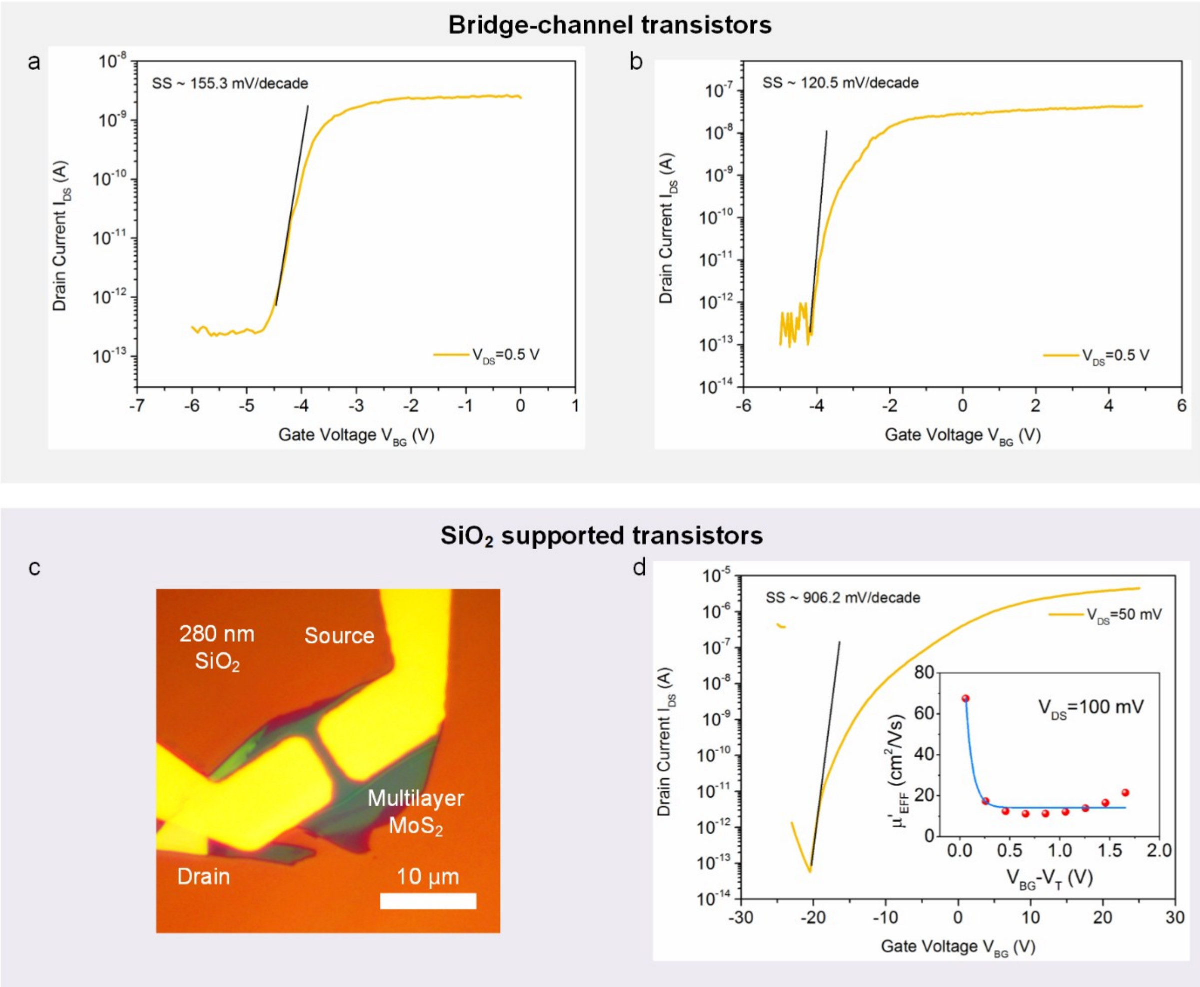

Fig. S8. Log scale of the transfer characteristics (I_{DS}-V_{BG}) for the bridge-channel devices with 1 nm-thick MoS_2 channel (a) and 11 nm-thick MoS_2 channel (b) under the same bias condition. (c) Optical microscope image of the SiO_2-supported device. (d) I_{DS}-V_{BG} characteristics for the MoS_2 on SiO_2 transistor at V_{DS}= 50 mV (Inset: calculated intrinsic effective mobility as function of V_{BG}-V_T). Here, the observed SS parameter (~906.2 mVdecade^{-1}) is consistent with other reports.[6-8] A large subthreshold swing is attributed to the presence of the large amount of interface trap DOS, as discussed in Manuscript.

Temperature dependent transport characteristics

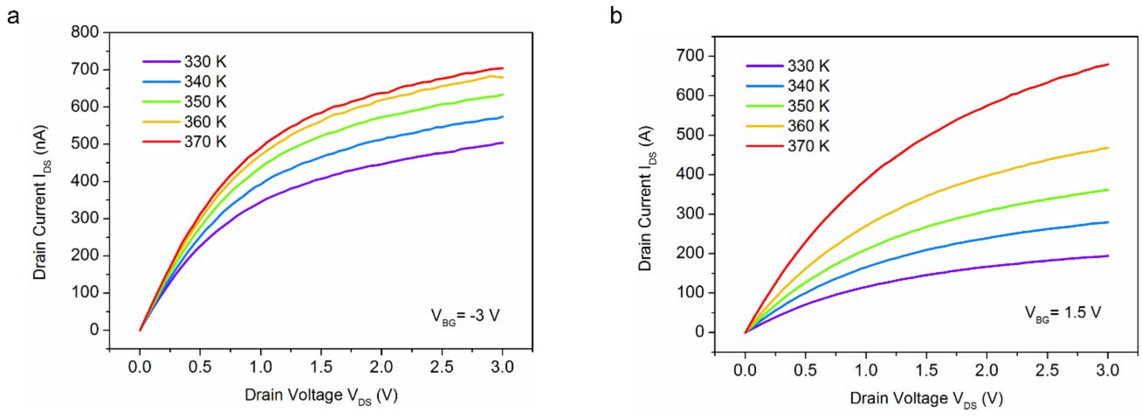

Fig. S9. Temperature-dependent transport characteristics for extraction activation energy. (a) I_{DS}-V_{DS} curves for the bridge-channel FET at temperature range from 330 K to 370 K with near threshold voltage gate bias (V_{BG}= -3 V). (b)) I_{DS}-V_{DS} curves for SiO_2-supported FET under the same condition (V_{BG}= 1.5 V).

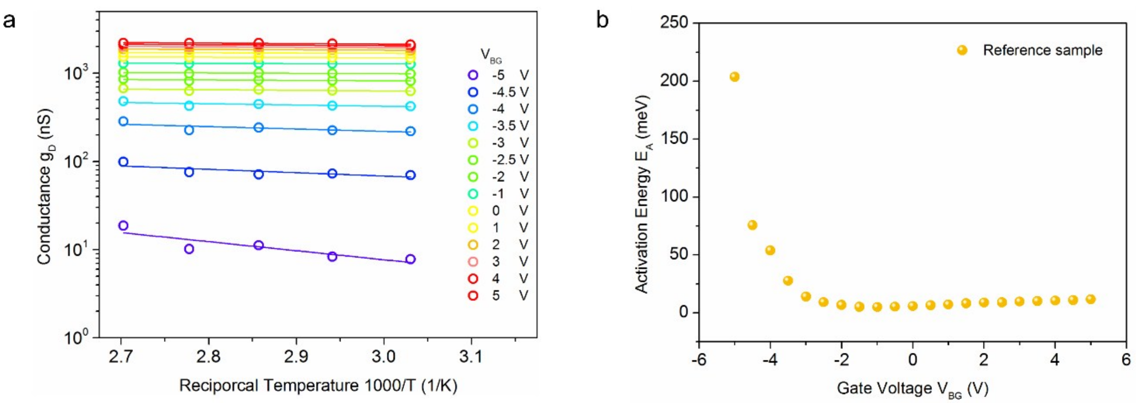

Fig. S10. (a) Arrhenius plot of the two-terminal conductance at various gate voltages. (b) The extracted activation energy data from (a). This reference sample was made by using PDMS transfer method and has the same device structure with Fig. 1a in Manuscript.

Reference

S1 C. Lee, H. Yan, L. E. Brus, T. F. Heinz, J. Hone and S. Ryu, *ACS Nano*, 2010, **4**, 2695-2700.

S2 H. Li, Q. Zhang, C. C. R. Yap, B. K. Tay, T. H. T. Edwin, A. Olivier and D. Baillargeat, *Adv. Funct. Mater.*, 2012, **22**, 1385-1390.

S3 S. Afrang, H. Mobki, M. H. Sadeghi and G. Rezazadeh, *Microelectron. Journal*, 2015, **46**, 191-197.

S4 D. K. Schroder, *Semiconductor material and device characterization*, John Wiley & Sons, 2006.

S5 S. Kim, A. Konar, W. S. Hwang, J. H. Lee, J. Lee, J. Yang, C. Jung, H. Kim, J. B. Yoo, J. Y. Choi, Y. W. Jin, S. Y. Lee, D. Jena, W. Choi and K. Kim, *Nat. Commun.*, 2012, **3**, 1011.

S6 K. Choi, Y. T. Lee, S. W. Min, H. S. Lee, T. Nam, H. Kim and S. Im, *J.Mater. Chem. C*, 2013, **1**, 7803-7807.

S7 J. Na, M.-K. Joo, M. Shin, J. Huh, J.-S. Kim, M. Piao, J.-E. Jin, H.-K. Jang, H. J. Choi and J. H. Shim, *Nanoscale*, 2014, **6**, 433-441.

S8 M. Y. Chan, K. Komatsu, S.-L. Li, Y. Xu, P. Darmawan, H. Kuramochi, S. Nakaharai, A. Aparecido-Ferreira, K. Watanabe and T. Taniguchi, *Nanoscale*, 2013, **5**, 9572-9576.